Solvation of Copper Ions by Acetonitrile. Structures and Sequential Binding Energies of $Cu^+(CH_3CN)_x$, $x = 1-5$, from Collision-Induced Dissociation and Theoretical Studies

G. Vitale, A. B. Valina, H. Huang, R. Amunugama, and M. T. Rodgers*

Department of Chemistry, Wayne State University, Detroit, Michigan 48202

Received: August 20, 2001; In Final Form: October 12, 2001

Collision-induced dissociation of $Cu^+(CH_3CN)_x$, $x = 1-5$, with xenon is studied as a function of kinetic energy using guided ion beam mass spectrometry. In all cases, the primary and lowest energy dissociation channel observed is endothermic loss of one acetonitrile molecule. The cross section thresholds are interpreted to yield 0 and 298 K bond energies after accounting for the effects of multiple ion-molecule collisions, internal energy of the complexes, and dissociation lifetimes. Density functional calculations at the B3LYP/6-31G* level of theory are used to determine the structures of these complexes and provide molecular constants necessary for the thermodynamic analysis of the experimental data. Theoretical bond dissociation energies are determined from single point calculations at the B3LYP/6-311+G(2d,2p) level and also with an extended basis on Cu^+ of 6-311+G(3df) using the B3LYP/6-31G* optimized geometries. The experimental bond energies determined here are in excellent agreement with previous experimental measurements made in a high-pressure mass spectrometer for the sum of the first and second bond energy (i.e., $Cu^+(CH_3CN)_2 \rightarrow Cu^+ + 2CH_3CN$) when these results are properly anchored. Excellent agreement between theory and experiment is also found for the $Cu^+(CH_3CN)_x$, $x = 1$ and 2 clusters. Theory systematically underestimates the binding energy in the larger clusters such that higher levels of theory are necessary to adequately describe the very weak noncovalent interactions in these systems.

Introduction

It has long been recognized that nocovalent interactions between ions and neutral molecules can be strongly influenced by the solvent in which such interactions are examined. In general, the solvent significantly weakens electrostatic forces (and hydrogen bonding interactions when present) between ions and molecules by shielding and competing for their attractions. In contrast, gas-phase measurements of such interactions are free of solvent effects, thus allowing the direct determination of the strength of the intrinsic interactions involved. Quite often, the relative behavior in solution parallels that of the gas phase, but in some cases, a marked change in the relative binding affinities is observed. An early example of such behavior was observed for the gas-phase basicities of the methylamines. The relative basicities in the gas phase follow the order $NH_3 < CH_3NH_2 < (CH_3)_2NH < (CH_3)_3N$.[1−4] This order differs from that observed in aqueous solution, where the basicities follow the order $NH_3 < (CH_3)_3N < CH_3NH_2 < (CH_3)_2NH$. Since this first observation, numerous examples of solvent-induced selectivity on noncovalent interactions have been observed in a variety of systems. By measuring such noncovalent interactions both in solution and the gas phase, the influence of the solvent on such interactions can in principle be elucidated. Alternatively, insight into the influence of solvent on noncovalent interactions between an ion and a ligand can also be gained by considering the competition between the solvation of the ion and complexation of the ion by the ligand of interest, reaction 1:

$$M^+(Solvent)_x + Ligand \rightarrow M^+(Ligand) + xSolvent \quad (1)$$

Thus, accurate gas-phase measurements of binding energies between ions and various ligands combined with analogous measurements of solvation enthalpies can be used to provide a better understanding of such interactions in solution. A particularly important aspect of such gas-phase studies is that the measurement of solvation enthalpies of ions can be potentially useful in the study of a wide variety of ligands. This provides motivation for the work performed here as well as a series of related studies currently being performed in our laboratory in which the solvation enthalpies of a variety of metal ions are being examined to commonly used solvents.[5]

An extensive number of studies of the solvation enthalpies of metal ions to water have been conducted.[6−26] Studies of the solvation enthalpies of metal ions to other commonly used solvents such as CH_3OH,[20,26−34] C_2H_5OH,[20,26,31−33] CH_3CN,[5,20,26,35−37] $(CH_3)_2CO$,[20,25−27,34,38,39] and $(CH_3)_2SO$[20,26,35] have been much more limited in scope and, in many of the cases examined thus far, have only measured enthalpies for the first or the first and second solvent molecule. Because it is may be necessary to include more than one or two solvent molecules, it is desirable to have accurate quantitative measurements of the enthalpies of solvation for as many solvent molecules as can be conveniently and accurately determined.

In recent work, we have developed methods to allow the application of quantitative threshold collision-induced dissociation (CID) methods to obtain accurate thermodynamic information on increasingly large systems.[5,17,31−33,39−48] One of the driving forces behind these developments is our interest in applying such techniques to large systems such as those of biological relevance. In addition, we seek to perform accurate thermochemical measurements that provide absolute anchors for metal cation affinity scales over an ever-broadening range of energies and molecular systems. In the present study, we use guided ion beam mass spectrometry to collisionally excite

10.1021/jp0132432 CCC: $20.00
Published on Web 11/17/2001

$Cu^+(CH_3CN)_x$ clusters. The kinetic energy-dependent cross sections for the CID processes are analyzed using methods developed previously.[40] The analysis explicitly includes the effects of the internal and translational energy distributions of the reactants, multiple collisions, and the lifetime for dissociation. We derive $(CH_3CN)_{x-1}Cu^+-CH_3CN$, $x = 1-5$ bond dissociation energies (BDEs) for all of the complexes and compare these results to density functional calculations performed here. Comparison is also made to previous experimental measurements.[36]

Previous work aimed at determination of the thermodynamics of $M^+(CH_3CN)_x$ clusters has been carried out by several groups using a variety of techniques. Equilibrium measurements in a Fourier transform ion cyclotron resonance mass spectrometer (FT-ICR) were carried out to determine the binding energy of Li^+ to CH_3CN.[26] Equilibrium measurements in a high-pressure mass spectrometer (HPMS) have also been performed to determine the binding energies of $M^+(CH_3CN)_x$, $x = 2-5$ for Na^+ and $1-5$ for K^+, Rb^+, and Cs^+,[35] and the total binding energies of $Ag^+(CH_3CN)_2$,[20] and $Cu^+(CH_3CN)_2$.[36] In an earlier study, we have also measured the binding energies of $Na^+(CH_3CN)_x$, $x = 1-5$ by guided ion beam tandem mass spectrometry.[5] The binding energies of $Ag^+(CH_3CN)_x$, $x = 1$ and 2, were also recently measured by threshold CID in a triple quadrupole instrument.[37]

Experimental Section

General Procedures. Cross sections for collision-induced dissociation of $Cu^+(CH_3CN)_x$ clusters are measured using a guided ion beam mass spectrometer that has been described in detail previously.[45] The $Cu^+(CH_3CN)_x$ clusters are generated as described below. The ions are extracted from the source, accelerated, and focused into a magnetic sector momentum analyzer for mass analysis. Mass-selected ions are decelerated to a desired kinetic energy and focused into an octopole ion guide, which traps the ions in the radial direction.[49] The octopole passes through a static gas cell containing xenon, used as the collision gas, for reasons described elsewhere.[50-52] Low gas pressures in the cell (typically 0.05−0.20 mTorr) are used to ensure that multiple ion-molecule collisions are improbable. Product and unreacted beam ions drift to the end of the octopole, where they are focused into a quadrupole mass filter for mass analysis and subsequently detected with a secondary electron scintillation detector and standard pulse counting techniques.

Ion intensities are converted to absolute cross sections as described previously.[53] Absolute uncertainties in cross section magnitudes are estimated to be ±20%, which are largely the result of errors in the pressure measurement and the length of the interaction region. Relative uncertainties are approximately ±5%.

Ion kinetic energies in the laboratory frame, E_{lab}, are converted to energies in the center of mass frame, E_{CM}, using the formula $E_{CM} = E_{lab}m/(m + M)$, where M and m are the masses of the ionic and neutral reactants, respectively. All energies reported below are in the CM frame unless otherwise noted. The absolute zero and distribution of the ion kinetic energies are determined using the octopole ion guide as a retarding potential analyzer as previously described.[53] The distribution of ion kinetic energies is nearly Gaussian with a fwhm typically between 0.2 and 0.4 eV (lab) for these experiments. The uncertainty in the absolute energy scale is ±0.05 eV (lab).

Even when the pressure of the reactant neutral is low, it has previously been demonstrated that the effects of multiple collisions can significantly influence the shape of CID cross sections.[54] Because the presence and magnitude of these pressure effects is difficult to predict, we have performed pressure-dependent studies of all cross sections examined here. In the present systems, we observe small cross sections at low energies that have an obvious dependence upon pressure. We attribute this to multiple energizing collisions that lead to an enhanced probability of dissociation below threshold as a result of the longer residence time of these slower moving ions. Data free from pressure effects are obtained by extrapolating to zero reactant pressure, as described previously.[54] Thus, results reported below are due to single bimolecular encounters.

Ion Source. The $Cu^+(CH_3CN)_x$ clusters are formed in a 1−1.5 m long flow tube[45] operating at a pressure of 0.7−1.1 Torr with a helium flow rate of 4000−6000 sccm. Copper ions are generated in a continuous dc discharge by argon ion sputtering of a cathode made from copper. Typical, operating conditions of the discharge for copper ion production are 1.0−2.0 kV and 5−15 mA in a flow of roughly 10% argon in helium. The $Cu^+(CH_3CN)_x$ clusters are formed by associative reactions of the copper ion with acetonitrile molecules that are introduced into the flow 20−50 cm downstream from the dc discharge. The flow conditions used in this ion source provide in excess of 10^5 collisions between an ion and the buffer gas, which should thermalize the ions both vibrationally and rotationally. In our analysis of the data, we assume that the ions produced in this source are in their ground electronic states and that the internal energy of the $Cu^+(CH_3CN)_x$ clusters is well described by a Maxwell-Boltzmann distribution of ro-vibrational states at 300 K. Previous work from this[42,44-47] and the Armentrout laboratories has shown that these assumptions are generally valid.[50,54-58]

Thermochemical Analysis. The reaction cross sections for collision-induced dissociation are influenced by several factors (discussed under General Procedures in the Experimental Section and below) that shift the "apparent threshold" from the true thermodynamic threshold. To extract accurate thermochemical data from threshold CID studies, these factors must be explicitly included in the thermochemical analysis of experimental data. To properly account for such effects, the threshold regions of the reaction cross sections are modeled using eq 2

$$\sigma(E) = \sigma_0 \sum_i g_i (E + E_i - E_0)^n / E \qquad (2)$$

where σ_0 is an energy independent scaling factor, E is the relative translational energy of the reactants, E_0 is the threshold for reaction of the ground electronic and ro-vibrational state, and n is an adjustable parameter that describes the efficiency of collisional energy transfer.[59] The summation is over the ro-vibrational states of the reactant ions, i, where E_i is the excitation energy of each state and g_i is the population of those states ($\sum g_i = 1$). The populations of excited ro-vibrational levels are not negligible even at 298 K as a result of the many low-frequency modes present in these ions. The relative reactivity of all ro-vibrational states, as reflected by σ_0 and n, is assumed to be equivalent.

The Beyer-Swinehart algorithm[60] is used to evaluate the density of the ro-vibrational states, and the relative populations, g_i are calculated by an appropriate Maxwell-Boltzmann distribution at the 298 K temperature appropriate for the reactants. The average vibrational energy at 298 K of the $Cu^+(CH_3CN)_x$ clusters are also given in the Supplementary Information in Table S1. We have estimated the sensitivity of our analysis to the deviations from the true frequencies by scaling the calculated frequencies to encompass the range of average scaling factors needed to bring calculated frequencies into agreement with

experimentally determined frequencies found by Pople et al.[61] Thus, the originally calculated vibrational frequencies were increased and decreased by 10%. The corresponding change in the average vibrational energy is taken to be an estimate of one standard deviation of the uncertainty in vibrational energy (Table S1) and is included in the uncertainties, also reported as one standard deviation, listed with the E_0 values.

We also consider the possibility that collisionally activated complex ions do not dissociate on the time scale of our experiment (approximately 10^{-4} s, but energy-dependent) by including statistical theories for unimolecular dissociation, specifically Rice-Ramsperger-Kassel-Marcus (RRKM) theory, into eq 2 as described in detail elsewhere.[40,57] This requires sets of ro-vibrational frequencies appropriate for the energized molecules and the transition states (TSs) leading to dissociation. The former sets are given in the Supplementary Information in Tables S1 and S2, whereas we assume that the TSs are loose and product-like because the interaction between the copper ion and the acetonitrile molecules is largely electrostatic. In this case, the TS vibrations used are the frequencies corresponding to the products, which are also found in Table S1. The transitional frequencies, those that become rotations and translations of the completely dissociated products, are treated as rotors, a treatment that corresponds to a phase space limit (PSL) and is described in detail elsewhere.[40] Two of the rotors are simply the two rotational constants of the CH_3CN product with axes that are perpendicular to the reaction coordinate and correspond to the its 2D rotational constant (0.31 cm^{-1}). In the $Cu^+(CH_3CN)$ system, which yields one atomic product, these are the only two transitional modes. For the larger clusters, three additional transitional modes exist. Two of these rotors are the rotational constants of the $Cu^+(CH_3CN)_{x-1}$ product, again those that are perpendicular to the reaction coordinate. Of the two rotational constants of the products with axes lying along the reaction coordinate, one is a transitional mode and is assigned as the remaining rotational constant of the CH_3CN product (5.29 cm^{-1}). The other becomes the 1-D external rotor of the TS. These are listed in Table S2. The external rotations of the energized molecule and TS are also included in the modeling of the CID data. The external rotational constants of the TS are determined by assuming that the TS occurs at the centrifugal barrier for interaction of $Cu^+(CH_3CN)_{x-1}$ with the neutral CH_3CN molecule, calculated variationally as outlined elsewhere.[40] The 2-D external rotations are treated adiabatically but with centrifugal effects included, consistent with the discussion of Waage and Rabinovitch.[62] In the present work, the adiabatic 2-D rotational energy is treated using a statistical distribution with explicit summation over the possible values of the rotational quantum number, as described in detail elsewhere.[3]

The model represented by eq 2 is expected to be appropriate for translationally driven reactions[63] and has been found to reproduce reaction cross sections well in a number of previous studies of both atom-diatom and polyatomic reactions,[64,65] including CID processes.[5,50,54,56,57,66−68] The model is convoluted with the kinetic energy distributions of both the reactant cluster ion and neutral xenon atom, and a nonlinear least-squares analysis of the data is performed to give optimized values for the parameters σ_0, E_0, and n. The error associated with the measurement of E_0 is estimated from the range of threshold values determined for different zero-pressure extrapolated data sets, variations associated with uncertainties in the vibrational frequencies, and the error in the absolute energy scale, 0.05 eV (lab). For analyses that include the RRKM lifetime effect, the uncertainties in the reported E_0 values also include the effects of increasing and decreasing the time assumed available for dissociation (or equivalently, the distance traveled between the collision and detection) by a factor of 2.

Equation 2 explicitly includes the internal energy of the ion, E_i. All energy available is treated statistically, which should be a reasonable assumption because the internal (rotational and vibrational) energy of the reactants is redistributed throughout the ion upon impact with the collision gas. The threshold for dissociation is by definition the minimum energy required leading to dissociation and thus corresponds to formation of products with no internal excitation. The assumption that products formed at threshold have an internal temperature of 0 K has been tested for several systems.[31−33,50,51,56,57] It has also been shown that treating all energy of the ion (vibrational, rotational, and translational) as capable of coupling into the dissociation coordinate leads to reasonable thermochemistry. The threshold energies for dissociation reactions determined by analysis with eq 2 are converted to 0 K bond energies by assuming that E_0 represents the energy difference between reactants and products at 0 K.[69] This assumption requires that there are no activation barriers in excess of the endothermicity of dissociation. This is generally true for ion-molecule reactions[64] and should be valid for the simple heterolytic bond fission reactions examined here.[70]

Density Functional Calculations. To obtain model structures, vibrational frequencies, rotational constants, and energetics for the neutral CH_3CN ligand and for the $Cu^+(CH_3CN)_x$ clusters, density functional calculations were performed using Gaussian 98.[71] Geometry optimizations were performed at the B3LYP/6-31G* level.[72,73] Vibrational analyses of the geometry-optimized structures were performed to determine the vibrational frequencies of the reactant and product cluster ions, $Cu^+(CH_3CN)_x$ and the neutral CH_3CN molecule. When used to model the data or to calculate thermal energy corrections, the B3LYP/6-31G* vibrational frequencies are scaled by a factor of 0.9804.[74] The scaled vibrational frequencies thus obtained for the systems studied are available as Supporting Information and listed in Table S1, while Table S2 lists the rotational constants. Single-point energy calculations were performed at the B3LYP/6-311+G(2d,2p) level, and with an extended basis set of B3LYP/6-311+G(3df) on Cu^+ using the B3LYP/6-31G* optimized geometries. To obtain accurate bond dissociation energies, zero-point energy (ZPE) corrections were applied and basis set superposition errors (BSSE) were subtracted from the computed dissociation energies in the full counterpoise approximation.[75,76] The ZPE corrections are small and vary with the size of the cluster, and are 4.2, 4.4, 2.6, 2.1, and 2.9 kJ/mol for the $Cu^+(CH_3CN)_x$ clusters, $x = 1-5$, respectively. Similarly, the BSSE corrections are small and range from 0.5 to 3.0kJ/mol but are slightly larger and range from 0.5 to 3.2 kJ/mol for the calculations with the extended basis set on Cu^+.

Results

Cross Sections for Collision-Induced Dissociation. Experimental cross sections are shown in Figure 1 for the interaction of $Cu^+(CH_3CN)_x$, $x = 1-5$ clusters with xenon. The sequential loss of intact acetonitrile molecules and ligand exchange with xenon are the only processes observed in these systems over the collision energy range studied, typically 0 to >10.0 eV. The primary (most favorable) process for all clusters is the loss of a single acetonitrile molecule in the CID reaction 3:

$$Cu^+(CH_3CN)_x + Xe \rightarrow Cu^+(CH_3CN)_{x-1} + CH_3CN + Xe \quad (3)$$

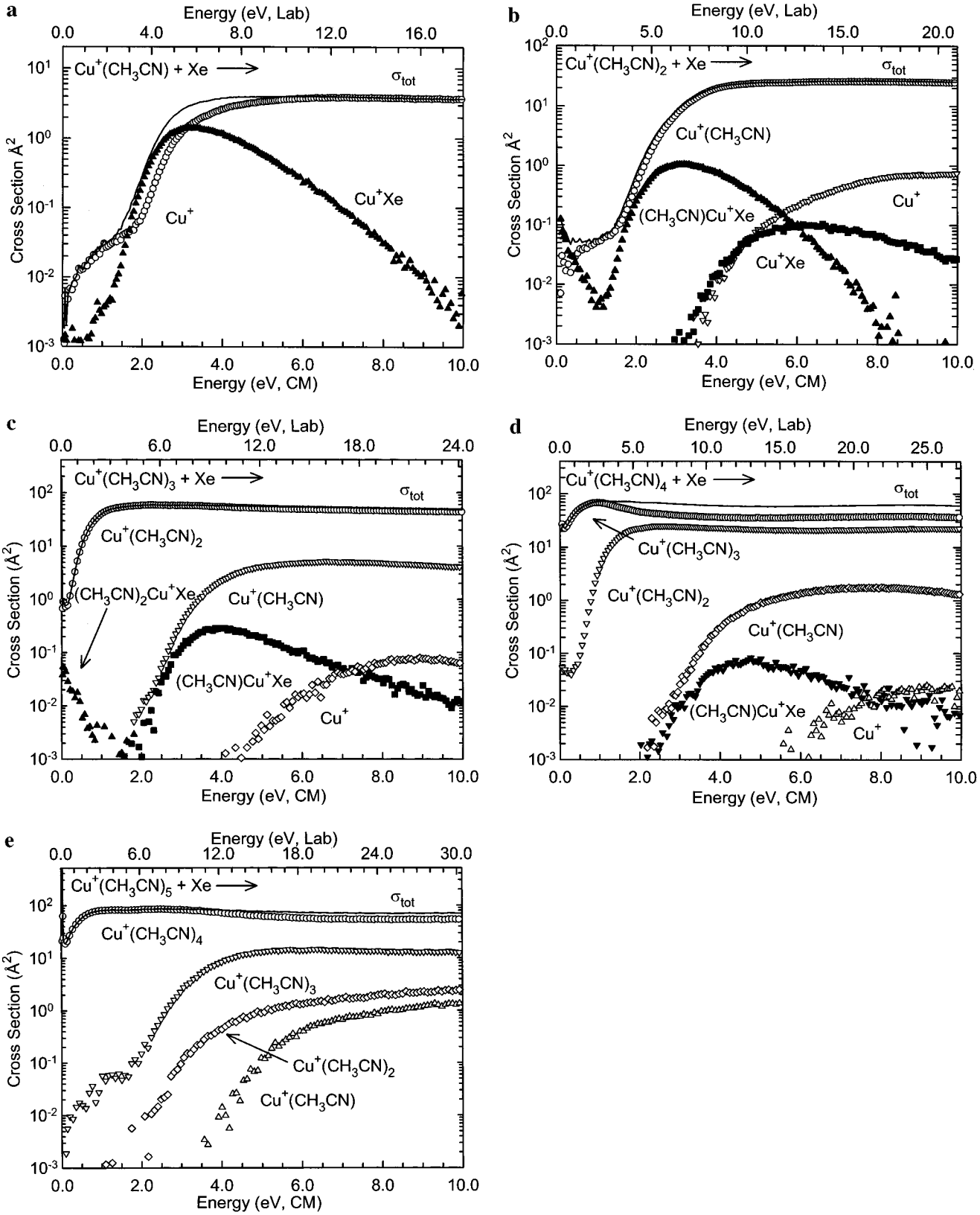

Figure 1. Cross sections for the collision-induced dissociation of the $Cu^+(CH_3CN)_x$, $x = 1-5$ (parts a−e, respectively), with Xe as a function of the kinetic energy in the center-of-mass frame (lower *x*-axis) and laboratory frame (upper *x*-axis). Data are shown for a Xe pressure of ∼0.2 mTorr. Primary, secondary, tertiary, and quaternary product cross sections are shown as ○, ▽, ◇, and △, respectively. Primary, secondary, and tertiary ligand exchange product cross sections are shown as ▲, ■, and ▼, respectively.

As the size of the cluster increases, the maximum cross section for reaction 3 (as well as the total cross section) increases in magnitude in a manner roughly consistent with the percentage increase in ligands. As the size of the cluster increases, the threshold for reaction 3 decreases, consistent with conventional ideas of ligation of gas-phase ions; i.e., stepwise sequential bond energies decrease because of increasing electrostatic repulsion between the ligands, causing the distance between the cation

and ligands to increase. Such ideas have been noted in previous experimental and theoretical studies of $M^+(ligand)_n$ clusters.[7,15,35,77]

Dissociation of additional CH_3CN ligands is observed for the larger clusters. For $x \geq 2$, loss of a second CH_3CN molecule is observed at higher energies. For $x \geq 3$, loss of a third CH_3CN molecule is observed at even higher energies. For $x \geq 4$, loss of a fourth CH_3CN molecule is observed at even higher energies. For $x = 5$, loss of a fifth CH_3CN molecule is not observed over the energy range examined here. As the size of the cluster increases, secondary, tertiary, and quaternary dissociation generally account for greater percentages of the total cross section, approximately 3%, 8%, 39%, and 24% for $x = 2-5$, respectively, at the highest energies examined. The decrease in percentage contribution to the total cross section for the $Cu^+(CH_3CN)_5$ cluster is unexpected and somewhat difficult to understand. It may arise from the differences in the nature of the binding of the fifth CH_3CN molecule, i.e., second solvent shell versus first solvent shell. As a result of the greater accessibility of this ligand, it might carry off more energy upon dissociation, thereby decreasing the likelihood of sequential dissociation of the $Cu^+(CH_3CN)_4$ product ion.

The cross sections for ligand exchange decrease as the size of the cluster increases. For the case of $x = 1$, the cross section for the ligand exchange process is substantial, having a maximum nearly 35% as large as the CID process. Although the magnitude of the ligand exchange cross section for the $x = 2$ cluster is nearly as large as it is for the $x = 1$ cluster, its contribution to the total cross section has dropped by nearly 1 order of magnitude, such that it accounts for less than 5% of the total cross section. Similarly, the ligand exchange cross sections continue to decrease with increasing solvation such that for the $x = 3$ and 4 clusters, the ligand exchange processes account for less than 0.5% and 0.1% of the total cross section. For the $x = 5$ cluster, the efficiencies of the ligand exchange processes have decreased enough that it could not be measured for this cluster.

$Cu^+(CH_3CN)$ + Xe. Results for the interaction of $Cu^+(CH_3CN)$ with xenon are shown in Figure 1a. The major product is Cu^+. The cross section for this process exhibits a small feature (<1%) at low energies that is not removed by pressure extrapolation and which we attribute to a small amount of Cu^+ in its first excited state (s^1d^9, ^3D) that has not been completely quenched in the flow tube source. The presence of this feature slightly complicates the analysis of the data, but as will be discussed below, it does not appear to influence the accuracy of our determination of the binding energy in this system. Ignoring this low energy feature, the Cu^+ product cross section has an apparent threshold of 1.2 eV and a maximum cross section of ~4 Å^2. The ligand exchange product Cu^+Xe is observed with an apparent threshold of 1.0 eV and a maximum cross section of 1.4 Å^2 at 3.2 eV, which drops off rapidly with energy due to competition with the primary CID process. Because the Cu^+Xe ligand exchange product cross section has a lower threshold than the Cu^+ product and a modest magnitude, it seems plausible that the apparent threshold for the CID process may be shifted to energies higher than the true thermodynamic threshold by competition with this ligand exchange process, a competitive shift. We do not believe this is a problem in this system, as the threshold measured here for the CID process is in good agreement with the theoretical values calculated, as will be discussed below. Within the quoted experimental errors, we do not believe such competition is likely to affect our threshold measurements in any of these systems for several reasons that have been detailed elsewhere.[68]

$Cu^+(CH_3CN)_2$ + Xe. Results for the interaction of $Cu^+(CH_3CN)_2$ with xenon are shown in Figure 1b. The major product is $Cu^+(CH_3CN)$. The cross section for this process also exhibits a small feature (<0.3%) at low energies that is not removed by pressure extrapolation and which we again attribute to a small amount of Cu^+ in its first excited state (s^1d^9, ^3D) that has not been completely quenched in the flow tube source. The presence of this feature slightly complicates the analysis of the data, but again, it does not appear to influence the accuracy of our determination of the binding energy in this system. The loss of one acetonitrile molecule from this species begins at an apparent threshold near 0.8 eV and exhibits a maximum cross section of ~26 Å^2, more than twice as large as that of the monoligated ion. The secondary product of this reaction, Cu^+, has an apparent threshold of ~3.6 eV. The Cu^+ product reaches a maximum cross section of ~0.1 Å^2 at the highest energies examined. Two ligand exchange products are observed, $(CH_3CN)Cu^+Xe$ and Cu^+Xe. The primary ligand exchange product, $(CH_3CN)Cu^+Xe$, exhibits a small exothermic feature at low energies arising from the minor contamination of the beam by $Cu^+(CH_3CN)_2$ in its first excited state. At higher energies, the ligand exchange cross section rises from an apparent threshold near 1.0 eV to a maximum of 1.0 Å^2 at approximately 3.2 eV. At higher energies, it falls off rapidly due to competition with the primary CID process. The secondary ligand exchange product, Cu^+Xe, slowly grows in from an apparent threshold near 3.3 eV to a maximum of 0.1 Å^2 at approximately 6.2 eV. At higher energies, it falls off due to competition with the secondary CID process.

$Cu^+(CH_3CN)_3$ + Xe. Results for the interaction of $Cu^+(CH_3CN)_3$ with xenon are shown in Figure 1c. The CID behavior for the triply ligated Cu^+ is notably different from that of the doubly ligated ion. The major product is $Cu^+(CH_3CN)_2$. The primary difference observed in the CID of this system is that the loss of one acetonitrile molecule from the reactant cluster begins at an apparent threshold near 0 eV with a cross section that is more than twice as large at its maximum as the maximum observed for the loss of one acetonitrile molecule from the doubly ligated ion. The cross section for production of the primary product decreases as the secondary $Cu^+(CH_3CN)$ product appears. The threshold for the secondary product appears at ~1.5 eV with a maximum cross section of ~5.2 Å^2 and then drops off slowly as the tertiary product, Cu^+, grows in from an apparent threshold near 4.3 eV. The Cu^+ product reaches a maximum cross section of ~0.1 Å^2 at the highest energies examined. Two ligand exchange products are observed. The second notable difference exhibited in the CID behavior of this cluster is that the primary ligand exchange product, $(CH_3CN)_2Cu^+Xe$, exhibits an exothermic feature which falls off rapidly with increasing energy. The secondary ligand exchange product, $(CH_3CN)Cu^+Xe$, rises from an apparent threshold near 1.5 eV to a maximum of ~0.3 Å^2 at approximately 4.0 eV. At higher energies, it falls off due to competition with the secondary CID process. Signals arising from the tertiary ligand exchange product, Cu^+Xe, were sufficiently small that they were not discernible from noise.

$Cu^+(CH_3CN)_4$ + Xe. Results for the interaction of $Cu^+(CH_3CN)_4$ with xenon are shown in Figure 1d. The CID behavior for the quadruply ligated Cu^+ is similar to that observed for the triply ligated system, except that at higher energies the secondary, tertiary, and quaternary dissociation processes account for a greater percentage of the total cross

TABLE 1: Fitting Parameters of Eq 2, Threshold Dissociation Energies at 0 K, Kinetic Shifts, and Entropies of Activation at 1000 K of $Cu^+(CH_3CN)_x$, $x = 1-5$[a]

species	σ_0[b]	n[b]	E_0[c] (eV)	E_0 (PSL) (eV)	kinetic shift (eV)	$\Delta S^{\ddagger}$(PSL) (J mol^{-1} K^{-1})
$Cu^+(CH_3CN)$	5.5 (0.3)	1.2 (0.1)	2.48 (0.03)	2.47 (0.03)	0.01	29 (2)
$Cu^+(CH_3CN)_2$	35.0 (2.0)	1.3 (0.1)	2.83 (0.10)	2.47 (0.09)	0.36	32 (4)
$Cu^+(CH_3CN)_3$	62.4 (1.1)[d]	0.8 (0.1)[d]	0.96 (0.03)[d]	0.87 (0.02)[d]	0.09	37 (3)[d]
	63.4 (1.1)[e]	0.8 (0.1)[e]	0.97 (0.03)[e]	0.88 (0.02)[e]	0.09	37 (3)[e]
$Cu^+(CH_3CN)_4$	91.4 (2.6)[d]	0.7 (0.1)[d]	0.80 (0.03)[d]	0.69 (0.02)[d]	0.11	24 (6)[d]
	89.8 (2.4)[e]	1.1 (0.1)[e]	0.67 (0.03)[e]	0.59 (0.03)[e]	0.08	25 (6)[e]
$Cu^+(CH_3CN)_5$[f]	108.4 (4.5)[d]	0.9 (0.1)[d]	0.97 (0.03)[d]	0.62 (0.04)[d]	0.35	−10 (6)[d]
	106.6 (5.2)[e]	0.9 (0.1)[e]	0.96 (0.03)[e]	0.61 (0.04)[e]	0.35	−10 (6)[e]
$Cu^+(CH_3CN)_5$[g]	104.8 (3.9)[d]	0.9 (0.1)[d]	0.94 (0.03)[d]	0.48 (0.03)[d]	0.46	−12 (6)[d]
	102.7 (4.1)[e]	0.9 (0.1)[e]	0.94 (0.03)[e]	0.47 (0.04)[e]	0.47	−11 (6)[e]

[a] Uncertainties are listed in parentheses. [b] Average values for loose PSL transition state. [c] No RRKM analysis. [d] Average values obtained when fitting the total cross section. [e] Average values obtained when fitting the channel corresponding to the loss of one acetonitrile molecule. [f] Ground state structure. [g] Trigonal bipyramid structure.

section. The apparent threshold for the primary product, $Cu^+(CH_3CN)_3$ appears near 0 eV with a cross section that is ~15% greater than the triply ligated species at their respective maxima. The cross section for production of the primary product decreases slightly more rapidly than that for the triply ligated species beginning at the apparent threshold for the secondary $Cu^+(CH_3CN)_2$ product. The $Cu^+(CH_3CN)_2$ product has an apparent threshold of ~0.1 eV and a maximum cross section of ~25 Å^2, which drops off slowly as the tertiary product, $Cu^+(CH_3CN)$, grows in. The apparent threshold for the $Cu^+(CH_3CN)$ product occurs near 2.3 eV and reaches a maximum cross section of ~1.8 Å^2, which declines very slowly as the quaternary product, Cu^+, grows in. The apparent threshold for the Cu^+ product occurs near 6.0 eV and reaches a maximum cross section of ~0.02 Å^2 at the highest energies examined. Only one ligand exchange product was observed. The primary ligand exchange product, $(CH_3CN)_3Cu^+Xe$, and secondary ligand exchange product, $(CH_3CN)_2Cu^+Xe$, are not observed. The tertiary ligand exchange product, $(CH_3CN)Cu^+Xe$, rises from an apparent threshold near 2.3 eV to a maximum cross section of 0.08 Å^2 at approximately 4.8 eV. At higher energies, it falls off due to competition with the tertiary CID process. Signals arising from the quaternary ligand exchange product, Cu^+Xe, were sufficiently small that they were not discernible from noise.

$Cu^+(CH_3CN)_5$ + Xe. Results for the interaction of $Cu^+(CH_3CN)_5$ with xenon are shown in Figure 1e. The CID behavior for the quintuply ligated Cu^+ is similar to that observed for the cluster containing one less acetonitrile molecule. The apparent threshold for the primary product, $Cu^+(CH_3CN)_4$, appears near 0 eV with a cross section that is ~25% larger than the quadruply ligated species at their respective maxima. The cross section for production of the primary product decreases rapidly at the apparent threshold for the secondary $Cu^+(CH_3CN)_3$ product. The $Cu^+(CH_3CN)_3$ product has an apparent threshold of ~0.7 eV and a maximum cross section of ~15 Å^2, which drops off slowly as the tertiary product, $Cu^+(CH_3CN)_2$, grows in. The apparent threshold for the $Cu^+(CH_3CN)_2$ product occurs near 1.7 eV and reaches a maximum cross section of ~3 Å^2 at the highest energies examined. Although the $Cu^+(CH_3CN)_2$ product does not decline as the quaternary product, $Cu^+(CH_3CN)$, grows in, the rise in the cross section changes slope at the apparent threshold for this product. The apparent threshold for the $Cu^+(CH_3CN)$ product occurs near 3.5 eV and reaches a maximum cross section of ~1.4 Å^2 at the highest energies examined. The Cu^+ product, which is not expected to be formed very efficiently, is not observed over the range of energies examined. The ligand exchange product channels were all too small to be distinguished from noise.

Threshold Analysis. The model of eq 2 was used to analyze the thresholds for reactions 3 in all five $Cu^+(CH_3CN)_x$ systems. As previously discussed,[50,56,57] we believe the analysis of the primary CID thresholds provides the most reliable thermochemistry for such studies. This is because secondary and higher-order products are more sensitive to lifetime effects, and additional assumptions are needed to quantitatively include the multiple products formed. The results of these analyses are provided in Table 1. Two values of E_0 are listed: one without the RRKM lifetime analysis and one where the lifetime analysis is included (a loose PSL TS model). Comparison of the two E_0 values shows that the unimolecular dissociation rate and thus the kinetic shifts observed for these systems depend both upon the threshold energy and the number of acetonitrile molecules surrounding the copper ion. Thus dissociation of $Cu^+(CH_3CN)$ system exhibits a very small kinetic shift of 0.01 eV. The $Cu^+(CH_3CN)_2$ system exhibits of a much larger kinetic shift of 0.36 eV, while $Cu^+(CH_3CN)_x$, $x = 3-5$, exhibit kinetic shifts of 0.09, 0.11, and 0.35 eV, respectively. The total number of vibrations increases with the size of the cluster from 15 for $Cu^+(CH_3CN)$ to 87 for $Cu^+(CH_3CN)_5$. Likewise, the number of heavy atoms increases from 4 to 16 as the size of the cluster increases from one to five CH_3CN molecules. Thus, the number of low frequency vibrations, those resulting in the largest impact on the density of states and therefore lifetime of the dissociating cluster, increases with the size of the cluster. The density of states also increases with energy such that kinetic shifts increase with threshold energy. This implies that the observed kinetic shift should directly correlate with the size of the cluster ion and with the threshold energy. Thus, the kinetic shift observed in the $Cu^+(CH_3CN)_x$, $x = 3$ and 4 systems is smaller than that for $Cu^+(CH_3CN)_2$ as a result of the much weaker binding in these systems (Table 1).

Experimental cross sections and fits to the data using a loose PSL model are shown in Figure 2 for loss of a single acetonitrile molecule in the interaction of $Cu^+(CH_3CN)_x$, $x = 1-5$ clusters with Xe (reaction 3). In all cases, the experimental cross sections for reactions 3 are accurately reproduced using a loose PSL TS model.[40] Previous work has shown that this model provides the most accurate assessment of the kinetic shifts for CID processes for electrostatic ion-molecule complexes.[5,31−33,39−43,45,66,67] Good reproduction of the data is obtained over energy ranges exceeding 2.0 eV and cross section magnitudes of at least a factor of 100. For the $x = 4$ and 5 clusters, the cross sections are still finite at the lowest energies we examine, and hence, the reproduction does not cover quite the same magnitude range.

Two sets of fitting parameters are listed in Table 1 for the $Cu^+(CH_3CN)_x$, $x = 3$ and 4 clusters, and those obtained for the $x = 5$ cluster in which the molecular parameters used in data

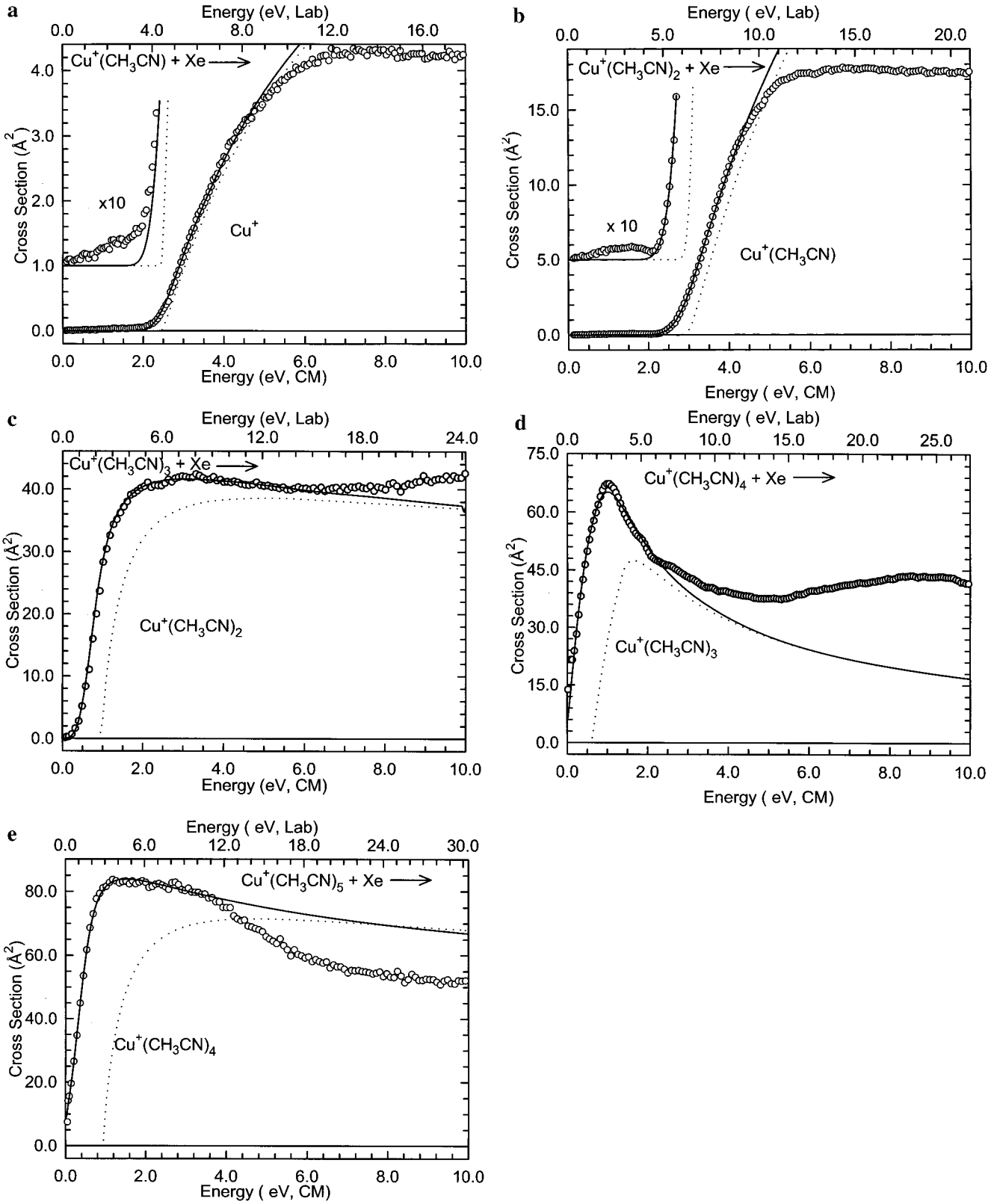

Figure 2. Zero-pressure-extrapolated primary product cross section for collision-induced dissociation of the $Cu^+(CH_3CN)_x$, $x = 1-5$ (parts a−e, respectively), with Xe in the threshold region as a function of kinetic energy in the center-of-mass frame (lower *x*-axis) and the laboratory frame (upper *x*-axis). A solid line shows the best fit to the data using eq 2 convoluted over the neutral and ion kinetic energy distributions. A dashed line shows the model cross sections in the absence of experimental kinetic energy broadening for reactants with an internal energy corresponding to 0 K.

analysis are derived from both the ground state and trigonal bipyramid structures. These represent analysis of the total cross section for dissociation and an analysis of the cross section for loss of a single acetonitrile molecule. Experimental cross sections and fits to the total CID cross section using a loose PSL TS model are shown in Figure 3 for the interaction of $Cu^+(CH_3CN)_x$, $x = 3-5$ clusters with Xe. For the $x = 1$ and 2 clusters, these two models give identical results. For the larger

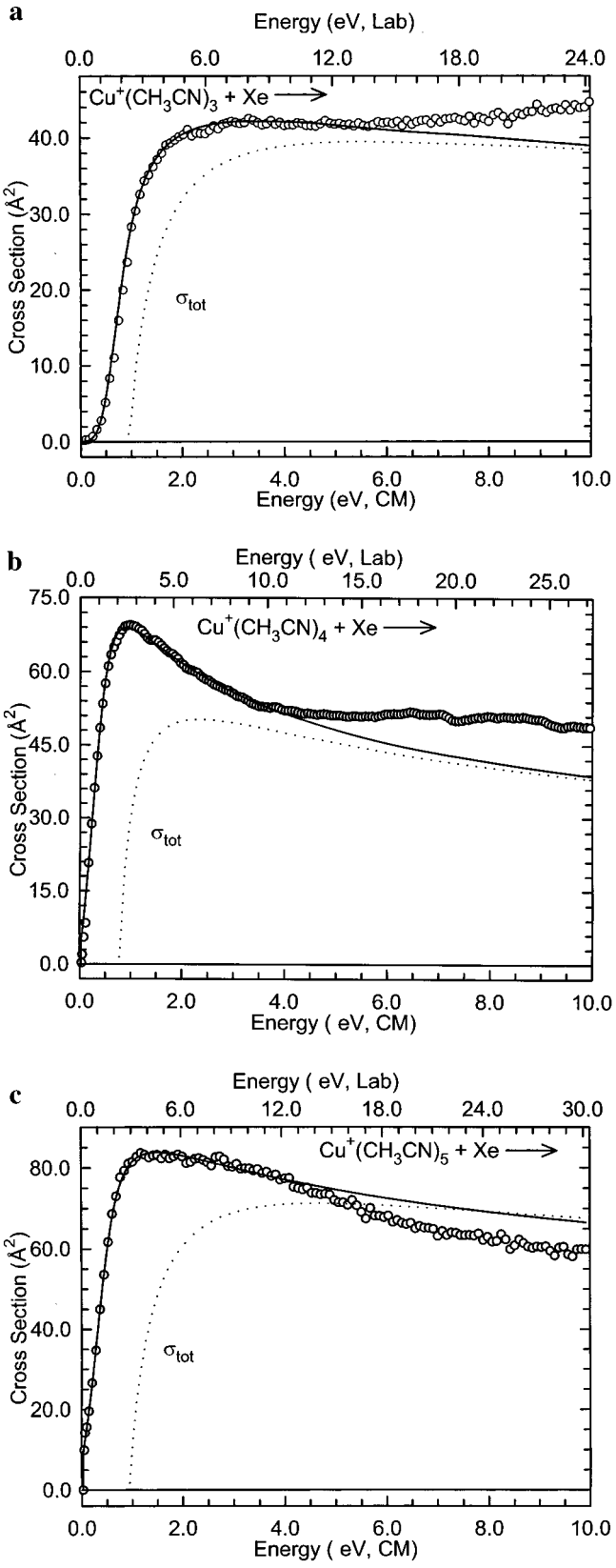

Figure 3. Zero-pressure-extrapolated total cross section for collision-induced dissociation of the $Cu^+(CH_3CN)_x$, $x = 3-5$ (parts a−c, respectively), with Xe in the threshold region as a function of kinetic energy in the center-of-mass frame (lower *x*-axis) and the laboratory frame (upper *x*-axis). A solid line shows the best fit to the data using eq 2 convoluted over the neutral and ion kinetic energy distributions. A dashed line shows the model cross sections in the absence of experimental kinetic energy broadening for reactants with an internal energy corresponding to 0 K.

clusters, $x = 3-5$, the fitting parameters obtained using the two models differ somewhat but result in threshold values that differ by only 0.01 eV in the $x = 3$ and 5 systems and by 0.10 eV for the $x = 4$ system. In these systems, the cross sections for reaction 3 are strongly affected by subsequent dissociation shortly after the threshold such that the energy range unaffected by this second-order process is narrow. As a result, the fits of the total cross section could be carried out over a more extensive energy range than those for the primary dissociation channel.

The entropy of activation, $\Delta S^{\ddagger}$, is a measure of the looseness of the TS and also a reflection of the complexity of the system. It is largely determined by the molecular parameters used to model the energized molecule and the TS but also depends on the threshold energy. Listed in Table 1, $\Delta S^{\ddagger}$(PSL) values at 1000 K show modest variation, as expected on the basis of the similarity of these systems. The entropy of activation ranges between 24 and 37 J K^{-1} mol^{-1} for the clusters containing 1−4 CH_3CN molecules. These entropies of activation can be favorably compared to a wide variety of noncovalently bound complexes previously measured in our laboratory and to the $\Delta S^{\ddagger}_{1000}$ values in the range of 29−46 J K^{-1} mol^{-1} collected by Lifshitz for several simple bond cleavage dissociations of ions.[78] The negative value obtained for the entropy of activation of the $Cu^+(CH_3CN)_5$ cluster is unexpected, as it the most weakly bound cluster and is expected to dissociation via a loose PSL TS. As mentioned above, this value is largely determined by the molecular parameters used to model the TS. In our analysis of the data, any negative frequencies calculated were found to correspond to the torsional motion of the CH_3 group and were replaced by a 1-D rotor with a rotational constant of 5.29 cm^{-1} (Table S2). There were no negative frequencies found for the $Cu^+(CH_3CN)_5$ cluster, whereas two were found for the $Cu^+(CH_3CN)_4$ product. This difference leads to the negative value for the entropy of activation found. If instead we treated all CH_3 torsions at 1-D rotors (5 for the reactant ion and 4 for the product ion), the entropy of activation becomes 42 J K^{-1} mol^{-1}. However, two of those CH_3 torsions are tied up by interaction with the fifth CH_3CN molecule. Therefore, it might be more accurate to treat only 3 of the CH_3 torsions in the reactant as 1-D rotors. In this case, the entropy of activation becomes 22 J K^{-1} mol^{-1}. In any event, the various treatments of the CH_3 torsional motions have very little influence upon the threshold for dissociation determined for this system and, thus, remains unchanged within the quoted experimental error.

Theoretical Results. Theoretical structures for the neutral CH_3CN ligand and for the $Cu^+(CH_3CN)_x$, $x = 1-5$ clusters were calculated as described above. Table 2 gives details of the final geometries for each of these species at the B3LYP/6-31G* level of theory. Two stable minima were found for the $Cu^+(CH_3CN)_5$ cluster. Results for the most stable conformation of the $Cu^+(CH_3CN)_x$, $x = 1-5$ clusters are shown in Figure 4, while Figure 5 shows the excited state conformation of $Cu^+(CH_3CN)_5$ cluster.[79]

As pointed out earlier,[35] aprotic solvents are characterized by a permanent dipole in which the positive charge is diffusely distributed over a large part of the molecule while the negative charge is concentrated in a small, accessible end of the molecule. This corresponds to the lone pair of electrons on the cyano nitrogen atom. Thus it is not surprising that the calculations find that the Cu^+ ion prefers to be bound to the lone pair of electrons on the cyano nitrogen atom along the axis of the molecule, rather than to the π-electrons of the C≡N bond. Attempts to calculate a stable $Cu^+(CH_3CN)$ complex in which Cu^+ binds to the π-electrons of the C≡N bond always

TABLE 2: B3LYP/6-31G* Geometry Optimized Structures of CH_3CN and $Cu^+(CH_3CN)_x$, $x = 1-5$[a]

	bond length (Å)				bond angle (°)				
species	Cu^+-N	C≡N	C−C	C−H	NCu^+N	Cu^+NC	NCC	CCH	HCH
CH_3CN	–	1.160	1.461	1.095	–	–	180.0	110.3	108.6
$Cu^+(CH_3CN)$	1.743	1.158	1.450	1.095	–	180.0	180.0	109.7	109.2
$Cu^+(CH_3CN)_2$	1.784	1.157	1.452	1.095	180.0	180.0	180.0	109.8	109.2
$Cu^+(CH_3CN)_3$	1.877	1.158	1.455	1.095	120.0	179.9	180.0	110.0	109.0
$Cu^+(CH_3CN)_4$	1.949	1.158	1.457	1.095	1.095	179.6	179.9	110.1	108.9
$Cu^+(CH_3CN)_5$[b]	1.941 (2)	1.158 (4)	1.457 (2)	1.095 (12)	113.1 (4)	179.7 (2)	179.9 (2)	110.1 (6)	109.4 (4)
	1.958 (2)	1.161 (1)	1.456 (2)	1.094 (3)	107.0 (1)	164.3 (2)	178.3 (2)	108.9 (2)	108.9 (6)
	5.747 (1)		1.461 (1)		97.4 (1)		180.0 (1)	110.2 (7)	108.8 (2)
									108.7 (2)
									108.4 (1)
$Cu^+(CH_3CN)_5$[c]	1.908 (3)	1.158 (3)	1.457 (3)	1.095 (3)	90.0 (6)	179.9	180.0	110.2	108.8
	2.252 (2)	1.159 (2)	1.461 (2)	1.094 (2)	120.0 (3)				
					179.7 (1)				

[a] Average values are provided when there exists more than one equivalent bond length or bond angle. [b] Ground state structure. [c] Trigonal bipyramid structure.

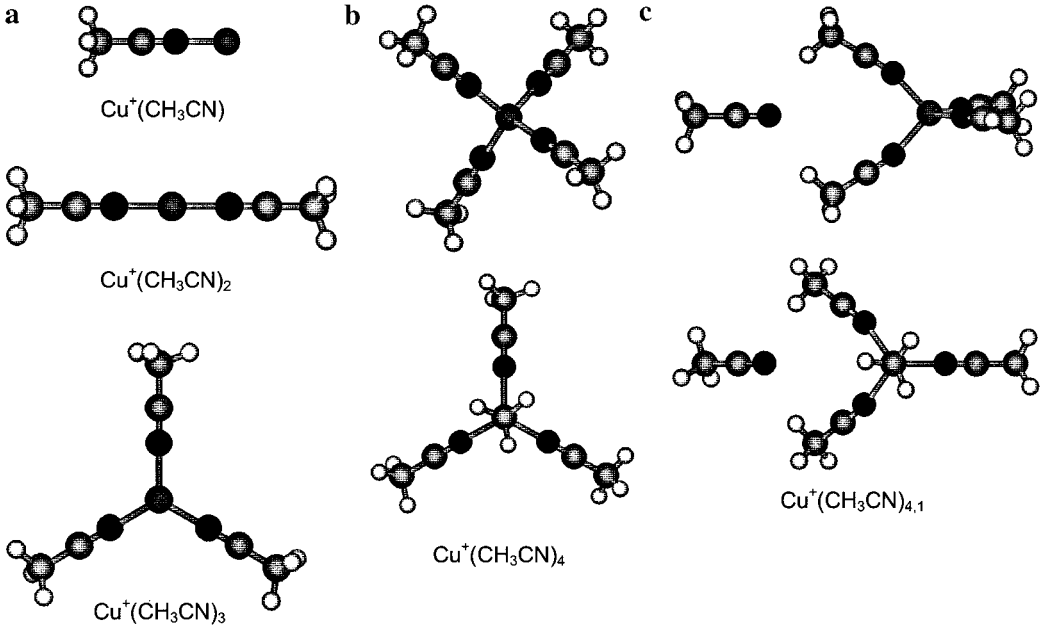

Figure 4. Optimized B3LYP/6-31G* ground state geometries of $Cu^+(CH_3CN)_x$, $x = 1-5$. The $x = 1-3$ structures are shown in part a, while two views of the $Cu^+(CH_3CN)_4$ and $Cu^+(CH_3CN)$ complexes are shown in parts b and c, respectively.

converged to the structure in which binding occurs to the lone pair of electrons on the cyano nitrogen atom. Thus, calculations of structures involving binding of Cu^+ to the π-electrons of the C≡N bond(s) were not pursued for the larger clusters. The distortion of the CH_3CN molecule that occurs upon complexation to the Cu^+ ion is very minor. The change in geometry is largest for the smallest cluster, $Cu^+(CH_3CN)$, and decreases with increasing number of solvent molecules. Bond lengths and bond angles change in the most extreme cases by less than 0.011 Å and 0.6°, respectively. The arrangement of the CH_3CN molecules around the copper ion in the $Cu^+(CH_3CN)_x$ clusters, $x = 1-4$, and the excited state conformer of the $Cu^+(CH_3CN)_5$ cluster is very nearly the ideal structures predicted by the valence shell electron pair repulsion (VSEPR) model, e.g., linear for $x = 1$ and 2, trigonal planar for $x = 3$, tetrahedral for $x = 4$, and trigonal bipyramidal for $x = 5$.[80] The Cu^+-N bond lengths increase as the number of CH_3CN molecules surrounding the Cu^+ ion increases. All of the Cu^+-N bond lengths are equivalent for the $x = 1-4$ clusters but become inequivalent for the $x = 5$ trigonal bipyramid structure. In this complex, the three CH_3CN molecules in the plane of the trigonal bipyramid are significantly closer to the Cu^+ ion than the two solvent molecules perpendicular to that plane, by almost 0.35 Å. Indeed, the Cu^+-N bond lengths for the equatorial ligands are actually shorter than they are in the $Cu^+(CH_3CN)_4$ tetrahedral complex, by 0.041 Å. A difference in these Cu^+-N bond lengths is expected on the basis of ligand-ligand repulsion in this complex; however, the magnitude of this is difference is somewhat surprising, as the analogous Na^+-N bond lengths differed by only 0.022 Å in the $Na^+(CH_3CN)_5$ cluster studied in our earlier work.[5] In addition, all of the Na^+-N bond lengths in the $x = 5$ cluster are longer than those in the $x = 4$ cluster. This marked difference in geometry likely arises from 4s−3d σ hybridization effects of the Cu^+ ion, as discussed below.

The crowding of five acetonitrile molecules in the first solvent shell as found by the theoretical calculations was predicted earlier by DK.[35] They suggested that the acetonitrile molecules would show a particularly strong tendency to crowd near the ion, i.e., in the first solvent shell. Removal of an acetonitrile molecule to the second solvent shell would increase the ion-solvent molecule distance significantly because acetonitrile is a long molecule. Furthermore, because of the aprotic nature of acetonitrile, bonding of an outer shell molecule to the inner shell molecules is expected to be very weak. In attempts to examine

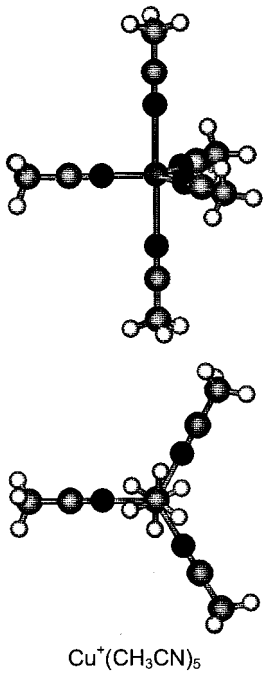

Figure 5. Optimized B3LYP/6-31G* geometry of a low-lying excited state conformer of the $Cu^+(CH_3CN)_5$ cluster. Two views of this trigonal bipyramidal cluster are shown.

such binding, we attempted calculations in which a fifth CH_3CN molecule was added to the second solvent shell of the $Cu^+(CH_3CN)_4$ complex. In the starting structure, the fifth CH_3CN molecule was positioned such that it occupied a 3-fold site in the second solvent shell. During the geometry optimization calculations, the fifth acetonitrile molecule wandered around for many iterations, with almost no change in the energy of the complex until it positioned itself such that gross changes in the geometry began to occur. Through multiple attempts, these calculations converged to the same trigonal bipyramid structure shown in Figure 5 with all five acetonitrile molecules in the first solvent shell of the complex. However, the trigonal bipyramid structure was calculated to be less stable than the $Cu^+(CH_3CN)_4 + CH_3CN$ dissociation asymptote, suggesting that the cluster with five acetonitrile molecules was not bound. This is obviously not the case, as we are able to produce a reasonably intense ion beam of this cluster at 298 K in our flow tube source. Thus, either the level of theory employedsignificantly underestimates the binding in this complex, or another stable structure exists. Further attempts to find another stable structure for the $Cu^+(CH_3CN)_5$ cluster eventually led to the ground-state structure for this complex shown in Figure 4c. To find this structure, the fifth acetonitrile molecule had to be placed in the second solvent shell aligned between two of the inner shell ligands. In this structure, four of the acetonitrile molecules occupy the first solvation shell in a distorted tetrahedral geometry, with the fifth acetonitrile molecule occupying a site in the second solvation shell that straddles two of the first solvent shell molecules. This structure is calculated to be 28.3 kJ/mol more stable than the trigonal bipyramid structure. Thus, for Cu^+, crowding of five acetonitrile molecules in the first solvent shell is less favorable than placing the fifth molecule in the second solvent shell despite the aprotic nature of acetonitrile. This behavior contrasts that found for the analogous Na^+ systems in which only a trigonal bipyramidal structure was found for the $Na^+(CH_3CN)_5$ cluster. This difference in the solvation behavior of Cu^+ versus Na^+ is probably a result of 4s−3d σ hybridization effects of the Cu^+ ion (which are not possible for Na^+), as discussed below.

Conversion from 0 to 298 K. To allow comparison to commonly used experimental conditions, we convert the 0 K bond energies determined here (experimentally and theoretically) to 298 K bond enthalpies and free energies. The enthalpy and entropy conversions are calculated using standard formulas (assuming harmonic oscillator and rigid rotor models) and the vibrational and rotational constants determined for the B3LYP/6-31G* optimized geometries, which are given in the Supporting Information in Tables S1 and S2. Table 3 lists 0 and 298 K enthalpy, free energy, and enthalpic and entropic corrections for all systems experimentally determined (from Table 1). Uncertainties in the enthalpic and entropic corrections are determined by 10% variation in the molecular constants. For the $Cu^+(CH_3CN)_x$ systems where the metal-ligand frequencies are very low and may not be adequately described by theory, the listed uncertainties also include scaling all frequencies below 150 cm^{-1} up and down by a factor of 2. The latter provides a conservative estimate of the computational errors in these low-frequency modes and is the dominant source of the uncertainties listed.

Discussion

Comparison of Theory and Experiment. The sequential BDEs for the $Cu^+(CH_3CN)_x$, $x = 1-5$ clusters at 0 K measured here by guided ion beam mass spectrometry are summarized in Table 4. Also listed here are the 0 K BDEs calculated at both the B3LYP/6-311+G(2d,2p)//B3LYP/6-31G* level, including zero point energy corrections and basis set superposition error corrections, and the same level of theory with an extended basis set on Cu^+ of B3LYP/6-311+G(3df).[81,82] The values for $x = 3-5$ represent the values obtained from fitting the total cross section. The agreement between theory and experiment is illustrated in Figure 6.

$Cu^+(CH_3CN)_x$, $x = 1-2$. The present results are the first direct measurements of the BDEs for the $Cu^+(CH_3CN)$ and $Cu^+(CH_3CN)_2$ complexes. As can be seen in Figure 6, excellent agreement between theory and experiment is found for these clusters. The theoretical BDE of $Cu^+(CH_3CN)$ lies 0.6 kJ/mol below the value measured here, well within the experimental error of this measurement (3.2 kJ/mol) and the expected accuracy of this level of theory. Similarly, the theoretical BDE of $Cu^+(CH_3CN)_2$ lies 3.9 kJ/mol below the value measured here. Again, this is well within the experimental error of this measurement (8.6 kJ/mol) and the expected accuracy of this level of theory. This suggests that the values measured here provide reliable assessments of the strength of the binding in these complexes. Another means of assessing the accuracy of the BDEs measured for these two clusters is to compare their sum to the value Deng and Kebarle[20] obtained for the total binding energy of the $Cu^+(CH_3CN)_2$ cluster.

In their work on the determination of bond energies of copper ion-ligand L complexes CuL_2^+, Deng and Kebarle[20] reported the free energies for the reaction, $CuL_2^+ = Cu^+ + 2L$ for some 23 different ligands which included CH_3CN. The values reported were derived from their measurements, as well as earlier measurements by Jones and Staley[83] and Magnera et al.[84] Deng and Kebarle reported a value for $\Delta G°_{393}$ for the above reaction when the ligand is CH_3CN of 357 kJ/mol. They converted this value to $\Delta H°_{298} = 454$ kJ/mol using appropriately scaled frequencies and rotational constants derived from ab initio calculations for CH_3CN and $Cu^+(CH_3CN)_2$ carried out at the HF/3-21G* level of theory. No error estimates were provided

TABLE 3: Enthalpies and Free Energies of Binding of $Cu^+(CH_3CN)_x$, $x = 1-5$, at 298 K in kJ/mol[a]

system	ΔH_0	$\Delta H_0{}^b$	$\Delta H_{298}-\Delta H_0{}^b$	ΔH_{298}	$\Delta H_{298}{}^b$	$T\Delta S_{298}{}^b$	ΔG_{298}	$\Delta G_{298}{}^b$
$Cu^+(CH_3CN)$	238.1 (3.2)	237.5	1.9 (1.1)	240.0 (3.4)	239.4	30.1 (2.8)	209.9 (4.4)	209.3
$Cu^+(CH_3CN)_2$	238.3 (8.6)	234.4	−0.2 (0.5)	238.1 (8.6)	234.2	39.2 (4.1)	198.9 (9.5)	195.0
$Cu^+(CH_3CN)_3$	84.1 (2.2)	67.9	0.0 (0.6)	84.1 (2.3)	67.9	36.2 (3.8)	47.9 (4.4)	31.7
$Cu^+(CH_3CN)_4$	67.0 (2.0)	45.1	−3.9 (1.5)	63.1 (2.5)	41.2	43.1 (10.4)	20.0 (10.7)	−1.9
$Cu^+(CH_3CN)_5{}^c$	59.9 (3.7)	20.4	−5.0 (1.7)	54.9 (4.1)	15.4	34.6 (13.8)	20.3 (14.4)	−19.2
$Cu^+(CH_3CN)_5{}^d$	46.5 (3.0)	−5.8	−2.2 (0.2)	44.3 (3.0)	−8.0	21.5 (7.6)	22.8 (8.0)	−29.5

[a] Uncertainties are listed in parentheses. [b] Density functional values from calculations at the B3LYP/6-311+G(2d,2p)//B3LYP/6-31G* level of theory with an extended basis set of B3LYP/6-311+G(3df) on Cu^+. [c] Ground state structure. [d] Trigonal bipyramid structure.

TABLE 4: Bond Dissociation Enthalpies of $Cu^+(CH_3CN)_x$, $x = 1-5$, at 0 K in kJ/mol

	experiment			theory (B3LYP)			
complex	TCID[a]	$D_e{}^b$	$D_0{}^{b,c}$	$D_{0,BSSE}{}^{b,d}$	$D_e{}^e$	$D_0{}^{c,e}$	$D_{0,BSSE}{}^{d,e}$
$Cu^+(CH_3CN)$	238.1 (3.2)	242.8	238.6	236.7	243.9	239.7	237.5
$Cu^+(CH_3CN)_2$	238.3 (8.6)	241.2	236.8	233.8	242.0	237.6	234.4
$Cu^+(CH_3CN)_3$	84.1 (2.2)	72.1	69.5	67.7	72.6	70.1	67.9
$Cu^+(CH_3CN)_4$	67.0 (2.0)	49.2	47.1	45.0	49.6	47.5	45.1
$Cu^+(CH_3CN)_5{}^f$	59.9 (3.7)	23.9	21.0	20.5	23.8	20.9	20.4
$Cu^+(CH_3CN)_5{}^g$	46.5 (3.0)	−4.2	−3.0	−5.1	−4.6	−3.3	−5.8

[a] Present results, threshold collision-induced dissociation. [b] Calculated at the B3LYP/6-311+G(2d,2p) level of theory using B3LYP/6-31G* optimized geometries. [c] Including zero point energy corrections with B3LYP/6-31G* frequencies scaled by 0.9804. [d] Also includes basis set superposition error corrections. [e] Calculated at the B3LYP/6-311+G(2d,2p) level of theory using B3LYP/6-31G* optimized geometries with an extended basis set of B3LYP/6-311+G(3df) for Cu. [f] Ground state structure. [g] Trigonal bipyramid structure.

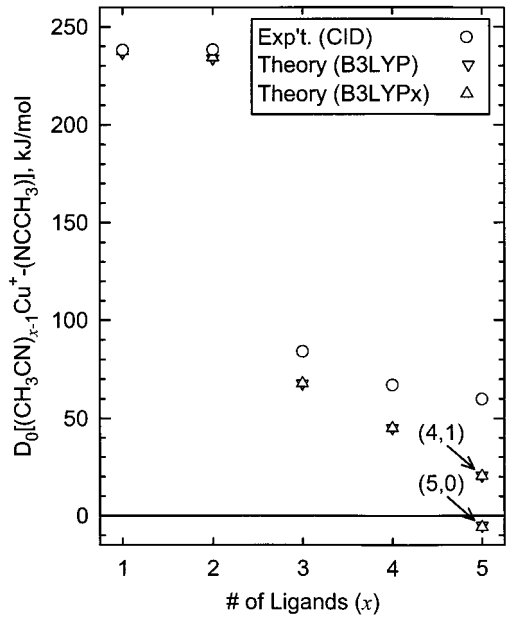

Figure 6. Experimental and theoretical bond energies at 0 K (in kJ/mol) of $[(CH_3CN)_{x-1}Cu^+-NCCH_3]$ plotted vs x. Two data points are provided for the $Cu^+(CH_3CN)_5$ cluster in which the trigonal bipyramidal conformer with all five CH_3CN molecules in the first solvent shell is designated (5, 0), and the ground state conformer with four CH_3CN molecules in the first solvent shell and one in the second solvent shell is designated (4, 1).

for these measurements, but their ladder of ΔG°_{393} values exhibited an internal consistency of better than 2 kJ/mol. To allow comparison to our results and others in the literature, we assume a conservative estimate of the error in their measurements of 4 kJ/mol. When this value is corrected to 0 K using the enthalpic thermal corrections provided in Table 3, their value becomes 453 ± 11 kJ/mol. Alternatively, their ΔG°_{393} value can be converted to 0 K using the results from our calculations for both the enthalpic (−0.6 ± 1.7 kJ/mol) and entropic corrections (91.9 ± 9.7 kJ/mol) at 393 K to give a 0 K enthalpy of 448 ± 11 kJ/mol. The difference in these values 5 kJ/mol is well within the estimated error (11.4 kJ/mol) of the thermal corrections or these measurements. However, Deng and Kebarle anchored their scale of Cu^+ binding affinities using theoretical values determined by Bauschlicher et al.[85] for $Cu^+(NH_3)_2$ because they believed that there were not any experimentally measured values available at that time. This was not the case, as Dalleska et al.[16] had previously measured the sequential BDEs of H_2O to the first-row transition-metal monocations by threshold CID techniques. If Dalleska et al.'s measured values for the $Cu^+(H_2O)_x$, $x = 1-2$ complexes are used to anchor the values reported by Deng and Kebarle, their ΔG°_{393} value for CH_3CN can be converted to a 0 K enthalpy of 477 ± 15 kJ/mol.[86] An alternative value can be derived from a study by Walter and Armentrout[87] (that appeared at about the same time that Deng and Kebarle's work appeared), in which they measured the sequential BDEs of NH_3 to the first-row transition-metal monocations by threshold CID techniques. If Walter and Armentrout's measured values for the $Cu^+(NH_3)_x$, $x = 1-2$ complexes are used to anchor the values measured by Deng and Kebarle, their ΔG°_{393} value for CH_3CN can be converted to a 0 K enthalpy of 505 ± 25 kJ/mol.[88] The analogous value for the total binding energy of $Cu^+(CH_3CN)_2$ derived from our results by summing the first and second BDEs gives a 0 K enthalpy of 476.4 ± 11.8 kJ/mol.

From this analysis, it seems clear that use of Bauschlicher's theoretical values for $Cu^+(NH_3)_x$ to anchor Deng and Kebarle's scale of Cu^+ binding affinities was inappropriate and results in absolute values that are too low. Additional support for this conclusion comes from the more accurate theoretical calculations performed here for these clusters. At the B3LYP/6-311+G(2d,2p)//B3LYP/6-31G* level of theory, the total binding energy of the $Cu^+(NH_3)_2$ is 8.5 kJ/mol greater than that calculated by Bauschlicher at al. Likewise, the use of Walter and Armentrout's values for $Cu^+(NH_3)_x$, $x = 1-2$ complexes to anchor Deng and Kebarle's scale of Cu^+ binding affinities results in absolute values that appear too high but which are still within the combined experimental errors of these measurements. Again, support for this conclusion comes from comparison of their values to the theoretical values determined here. The theoretical total binding energy we calculate for $Cu^+(NH_3)_2$ is 33.5 kJ/mol lower than that derived from their measurements. In

contrast, excellent agreement is achieved when Dalleska et al.'s values for $Cu^+(H_2O)_x$, $x = 1-2$ complexes are used to anchor Deng and Kebarle's scale of Cu^+ binding affinities. Additional support for the reliability of these measurements comes from comparison to the theoretical values determined here. The theoretical total binding energy we calculate for $Cu^+(H_2O)_2$ is only 9.2 kJ/mol lower than that derived from their measurements, well within the experimental error of these measurements. Thus internal consistency is achieved for the five studies involved (Jones and Staley,[83] Magnera et al.,[84] Deng and Kebarle,[20] Dalleska et al.,[16] and the present work) when the Cu^+ binding affinities are anchored in this way. As mentioned above, the values of Walter and Armentrout appear to be a little too high but are still within the combined experimental errors of these measurements. This suggests that the absolute values of Cu^+ binding affinities ($\Delta G°_{393}$) reported by Deng and Kebarle should be raised by ~29 kJ/mol and that the values reported by Dalleska et al. for $Cu^+(H_2O)_x$ or those reported here for $Cu^+(CH_3CN)_x$ provide accurate absolute values by which relative Cu^+ binding affinities might be anchored.

$Cu^+(CH_3CN)_x$, $x = 3-5$. The BDEs for $Cu^+(CH_3CN)_x$, $x = 3-5$, have not been previously measured. As can be seen in Figure 6, the theoretical BDEs for all clusters are consistently lower than the experimentally determined values. In fact, the deviation between the calculated and measured values increases with increasing size of the cluster such that the theoretical values are 16.2, 21.9, and 39.5 kJ/mol lower than the experimental values for $x = 3-5$, respectively. The binding energy of the trigonal bipyramid structure of $Cu^+(CH_3CN)_5$ deviates from the measured value by 52.3 kJ/mol.[89] In fact, theory suggests that the cluster with five acetonitrile molecules in this geometry is not bound with respect to the $Cu^+(CH_3CN)_4 + CH_3CN$ dissociation asymptote. The $Cu^+(CH_3CN)_5$ cluster is obviously bound, as we are able to produce a reasonably intense ion beam of this cluster at 298K in our flow tube source. This suggests that the structure of $Cu^+(CH_3CN)_5$ probed in our experiments must correspond to the ground state structure calculated. The observed agreement between theory and experiment seems quite reasonable, as it is be expected that the accuracy of theory should fall off with increasing solvation as a result of the very weak noncovalent interactions in the larger clusters requiring larger basis sets and higher levels of correlation to accurately describe these weak interactions. The lack of accuracy in the theoretical values for the larger clusters is what first motivated our calculations with an extended basis set on Cu^+ to provide more d-type orbitals to describe the weak interactions in these systems. However, the extended basis set only slightly improved the agreement between theory and experiment, by 0.8, 0.6, 0.2, and 0.1 kJ/mol, for the $x = 1-4$ clusters, respectively, and actually led to an increase in the deviation of 0.1 and 0.7 kJ/mol between theory and experiment for the $Cu^+(CH_3CN)_5$ clusters in the ground state and excited state trigonal bipyramidal structures, respectively. This suggests that higher levels of theory are necessary to obtain accurate theoretical values for these weakly bound clusters. The calculations performed here were very time consuming with the computational resources currently available to us and thus higher level calculations were not pursued.

Trends in the Sequential BDEs. The trends in the sequential BDEs of CH_3CN to Cu^+ can be contrasted with that measured for Na^+.[5] For Na^+, the BDEs decrease gradually as the number of solvent molecules increase. In contrast, the BDEs to Cu^+ for $x = 1$ and 2 are nearly equal and are much stronger than the corresponding BDEs to Na^+. A sharp decrease in the BDE occurs at $x = 3$, and then fairly small decreases are observed for the $x = 4$ and 5 clusters. Similar behavior has been observed in the solvation of Na^+ and Cu^+ by other ligand molecules.[16,85,87] This difference in the energetics of solvation for Cu^+ (and to varying extents for other transition metal ions) was first explained by Bauschlicher and co-workers.[85] They attributed the very strong bonds for the first two solvent molecules to the presence of 4s−3d σ hybridization of the metal orbital. 4s−3d σ hybridization hybridizes electron density away from the ligand in a direction perpendicular to the bonding axis. This allows the first two ligands to approach the metal ion with minimum electronic repulsion.

4s−3d σ hybridization effects continue to influence the larger clusters because additional ligands placed around the Cu^+ experience greater electron repulsion with the occupied 4s−3d σ orbital. This leads to much weaker BDEs for these ligands and also exerts a strong influence on the geometry of the larger clusters. As mentioned above the large difference in the Cu^+-N bond lengths for the equatorial and axial ligands of the trigonal bipyramid structure of $Cu^+(CH_3CN)_5$ probably arises from 4s−3d σ hybridization effects. The three equatorial ligands lie along the plane perpendicular to the occupied 4s−3d σ hybrid orbital and therefore experience minimum electron repulsion with this orbital. In contrast, the axial ligands lie along the direction of this occupied orbital and experience more electron repulsion resulting in longer Cu^+-N bond lengths. Likewise, the orientation of the fifth CH_3CN molecule in the ground-state $Cu^+(CH_3CN)_5$ cluster is likely stabilized by 4s−3d s hybridization effects. By aligning the fifth ligand in this way, electron density is minimized in the direction perpendicular to this ligand and the two opposing ligands; thus, electron repulsion between the ligands and the occupied 4s−3d s hybrid orbital is minimized.

Conclusions

The kinetic energy dependence of the collision-induced dissociation of $Cu^+(CH_3CN)_x$, $x = 1-5$, with Xe are examined in a guided ion beam mass spectrometer. The dominant dissociation process in all cases is loss of an intact CH_3CN ligand. Thresholds for these processes are determined after consideration of the effects of reactant internal energy, multiple collisions with Xe, and lifetime effects (using methodology described in detail elsewhere).[40] Insight into the structures and binding energies of the $Cu^+(CH_3CN)_x$ clusters is provided by density functional theory calculations of these complexes performed at the B3LYP/6-311+G(2d,2p)//B3LYP/6-31G* level of theory and at the same level of theory with an extended basis set of B3LYP/6-311+G(3df)z on Cu^+. The present results for all $Cu^+(CH_3CN)_x$ clusters represent the first direct measurement of the BDEs for these complexes. The total binding energy of the $Cu^+(CH_3CN)_2$ complex measured by Deng and Kebarle[20] (once properly anchored to the measured value for $Cu^+(H_2O)_2$ by Dalleska et al.[16]) is in excellent agreement with the value derived from our measurements. Excellent agreement between theory and experiment is obtained for the $Cu^+(CH_3CN)$ and $Cu^+(CH_3CN)_2$ complexes, suggesting that this ligand can act as another reliable anchor for the copper ion affinity scale, thus broadening the range of ligands available as absolute thermochemical anchors. It should be noted that the values reported by Deng and Kebarle[20] were anchored to theoretical values determined by Bauschlicher and co-workers[85] rather than to experimentally measured values. The values they reported should be correctly anchored to the values measured by Armentrout and co-workers for H_2O[16] or to the values measured here for CH_3CN. The agreement between theory and experiment varies with the size of the cluster. The reliability of theory

decreases with increasing cluster size, as it is expected that additional basis functions or greater levels of electron correlation are needed to accurately describe the very weak binding in the larger clusters. The theoretical calculations predict a surprising result for the $Cu^+(CH_3CN)_5$ cluster, where it is found that it is more favorable for the fifth solvent molecule to occupy a site in the second solvation shell rather than crowding into the first solvent shell despite the aprotic nature of acetonitrile.

Supporting Information Available: Tables of vibrational frequencies, average vibrational energies, and rotational constants for the B3LYP/6-31G* geometry optimized structures for neutral CH_3CN, and $Cu^+(CH_3CN)_x$ clusters, $x = 1-5$ (PDF). This material is available free of charge via the Internet at http://pubs.acs.org.

Acknowledgment. This work was supported in part by an ASMS Research Award from Micromass. A.B.V. thanks the MARC program for support under NIH Grant #5T34-GM08030-19 to Wayne State University.

References and Notes

(1) Munson, M. J. B. *J. Am. Chem. Soc.* **1965**, *87*, 2332.
(2) Beauchamp, J. L.; Butrill, S. E. *J. Chem. Phys.* **1968**, *48*, 1783.
(3) Brauman, J. I.; Blair, L. K. *J. Am. Chem. Soc.* **1968**, *90*, 5636.
(4) Brauman, J. I.; Riveros, J. M.; Blair, L. K. *J. Am. Chem. Soc.* **1971**, *93*, 3914.
(5) Valina, A. B.; Amunugama, R.; Huang, H.; Rodgers, M. T. *J. Phys. Chem. A*, in press.
(6) Searles, S. K.; Kebarle, P. *Can J. Chem*. **1969**, *47*, 2619.
(7) Dzidic, I.; Kebarle, P. *J. Phys. Chem*. **1970**, *74*, 1466.
(8) Davidson, W. R.; Kebarle, P. *J. Am. Chem. Soc*. **1976**, *98*, 6133.
(9) Peterson, K. I.; Holland, P. M.; Keesee, R. G.; Lee, N.; Mark, T. D.; Castleman, A. W. *Surf. Sci*. **1981**, *106*, 136.
(10) Castleman, A. W.; Peterson, K. I.; Upschulte, B. L.; Schelling, F. J. *Int. J. Mass Spectrom. Ion Phys*. **1983**, *47*, 203.
(11) Steel, E. A.; Merz, K. M.; Selinger, A.; Castleman, A. W. *J. Phys. Chem.* **1985**, *99*, 7829.
(12) Marinelli, P. J.; Squires, R. R. *J. Am. Chem. Soc*. **1989**, *111*, 4101.
(13) Schultz, R. H.; Armentrout, P. B. *J. Phys. Chem.* **1993**, *97*, 596.
(14) Dalleska, N. F.; Honma, K.; Armentrout, P. B. *J. Am. Chem. Soc*. **1993**, *115*, 12125.
(15) Dalleska, N. F.; Tjelta, B. L.; Armentrout, P. B. *J. Phys. Chem*. **1994**, *98*, 4191.
(16) Dalleska, N. F.; Honma, K.; Sunderlin, L. S.; Armentrout, P. B. *J. Am. Chem. Soc*. **1994**, *116*, 3519.
(17) Rodgers, M. T.; Armentrout, P. B. *J. Phys. Chem*. *A* **1997**, *101*, 1238.
(18) Peschke, M.; Blades, A. T.; Kebarle, P. *J. Phys. Chem. A* **1998**, *120*, 2925.
(19) Peschke, M.; Blades, A. T.; Kebarle, P. *J. Phys. Chem. A* **1998**, *102*, 9978.
(20) Deng, H.; Kebarle, P. *J. Phys. Chem. A* **1998**, *102*, 571.
(21) Rodriguez-Cruz, S. E.; Jockusch, R. A.; Williams, E. R. *J. Am. Chem. Soc*. **1998**, *120*, 5842.
(22) Rodriguez-Cruz, S. E.; Jockusch, R. A.; Williams, E. R. *J. Am. Chem. Soc*. **1999**, *121*, 1986.
(23) Rodriguez-Cruz, S. E.; Jockusch, R. A.; Williams, E. R. *J. Am. Chem. Soc*. **1999**, *121*, 8898.
(24) Nielsen, S. B.; Masella, M.; Kebarle, P. *J. Phys. Chem. A* **1999**, *103*, 9891.
(25) Peschke, M.; Blades, A. T.; Kebarle, P. *J. Am. Chem. Soc*. **2000**, *122*, 10440.
(26) Anvia, F.; Walsh, S.; Capon, M.; Koppel, I. A.; Taft, R. W.; de Paz, J. L. G.; Catalan, J. *J. Am. Chem. Soc.* **1990**, *112*, 5095. Taft, R. W.; Anvia, F.; Gal, J.-F.; Walsh, S.; Capon, M.; Holmes, M. C.; Hosn, K.; Oloumi, G.; Vasanwala, R.; Yazdani, S. *Pure Appl. Chem.* **1990**, *62*, 17. Burk, P.; Koppel, I. A.; Koppel, I.; Kurg, R.; Gal, J.-F.; Maria, P.-C.; Herreros, M.; Notario, R.; Abboud, J.-L. M.; Anvia, F.; Taft, R. W. *J. Phys. Chem. A* **2000**, *104*, 2824.
(27) Guo, B. C.; Conklin, B. J.; Castleman, A. W. *J. Am. Chem. Soc*. **1989**, *111*, 6506.
(28) Leuchtner, R. E.; Farley, R. W.; Harms, A. C.; Funasaka, H.; Castleman, A. W. *Int. J. Mass Spectrom. Ion Processes* **1990**, *102*, 199.
(29) Guo, B. C.; Castleman, A. W. *Int. J. Mass Spectrom. Ion Processes* **1990**, *100*, 665.
(30) Andersen, A.; Muntean, F.; Walter, D.; Rue, C.; Armentrout, P. B. *J. Phys. Chem. A* **2000**, *104*, 692.
(31) Rodgers, M. T.; Armentrout, P. B. *J. Phys. Chem. A* **1997**, *101*, 2614.
(32) Rodgers, M. T.; Armentrout, P. B. *J. Phys. Chem. A* **1999**, *103*, 4955.
(33) Rodgers, M. T.; Armentrout, P. B. *J. Chem. Phys*. **1998**, *109*, 1787.
(34) Hoyau, S.; Norrman, K.; McMahon, T. B.; Ohanessian, G. *J. Am. Chem. Soc*. **1999**, *121*, 8864.
(35) Davidson, W. R.; Kebarle, P. *J. Am. Chem. Soc*. **1976**, *98*, 6125.
(36) Deng, H.; Kebarle, P. *J. Am. Chem. Soc*. **1998**, *120*, 2925.
(37) Shoeib, T.; Houssain, E. A.; Siu, K. W. M.; Hopkinson, A. C. *J. Phys. Chem. A* **2001**, *105*, 710.
(38) Jarek, R. L.; Miles, T. D.; Trester, M. L.; Denson, S. C.; Shin, S. K. *J. Phys. Chem. A* **2000**, *104*, 2230.
(39) Armentrout, P. B.; Rodgers, M. T. *J. Phys. Chem. A* **2000**, *104*, 2238.
(40) Rodgers, M. T.; Ervin, K. M.; Armentrout, P. B. *J. Chem. Phys*. **1997**, *106*, 4499.
(41) Rodgers, M. T.; Armentrout, P. B. *Int. J. Mass Spectrom*. **1999**, *185*/*186*/*187*, 359.
(42) Amunugama, R.; Rodgers, M. T. *Int. J. Mass Spectrom*. **2000**, *195*/*196*, 439.
(43) Rodgers, M. T.; Armentrout, P. B. *J. Am. Chem. Soc*. **2000**, *122*, 8548.
(44) Rodgers, M. T.; Stanley, J. R.; Amunugama, R. *J. Am. Chem. Soc.* **2000**, *122*, 10969.
(45) Rodgers, M. T. *J. Phys. Chem. A* **2001**, *105*, 2374.
(46) Amunugama, R.; Rodgers, M. T. *J. Phys. Chem. A* **2001**, *105*, 9883.
(47) Rodgers, M. T. *J. Phys. Chem. A* **2001**, *105*, 8145.
(48) Rodgers, M. T.; Armentrout, P. B. *J. Am. Chem. Soc.*, submitted for publication.
(49) Teloy, E.; Gerlich, D. *Chem. Phys.* **1974**, *4*, 417. Gerlich, D. Diplomarbeit, University of Freiburg, Federal Republic of Germany, 1971. Gerlich, D. In *State-Selected and State-to-State Ion-Molecule Reaction Dynamics, Part I, Experiment*; Ng, C.-Y., Baer, M., Eds.; Advances in Chemical Physics series; Wiley: New York, 1992; Vol. 82, p 1.
(50) Dalleska, N. F.; Honma, K.; Armentrout, P. B. *J. Am. Chem. Soc.* **1993**, *115*, 12125.
(51) Aristov, N.; Armentrout, P. B. *J. Phys. Chem*. **1986**, *90*, 5135.
(52) Hales, D. A.; Armentrout, P. B. *J. Cluster Sci*. **1990**, *1*, 127.
(53) Ervin, K. M.; Armentrout, P. B. *J. Chem. Phys.* **1985**, *83*, 166.
(54) Dalleska, N. F.; Honma, K.; Sunderlin, L. S.; Armentrout, P. B. *J. Am. Chem. Soc*. **1994**, *116*, 3519.
(55) Schultz, R. H.; Armentrout, P. B. *J. Chem. Phys*. **1992**, *96*, 1046.
(56) Schultz, R. H.; Crellin, K. C.; Armentrout, P. B. *J. Am. Chem. Soc.* **1992**, *113*, 8590.
(57) Khan, F. A.; Clemmer, D. C.; Schultz, R. H.; Armentrout, P. B. *J. Phys. Chem*. **1993**, *97*, 7978.
(58) Fisher, E. R.; Kickel, B. L.; Armentrout, P. B. *J. Phys. Chem*. **1993**, *97*, 10204.
(59) Muntean, F.; Armentrout, P. B. *J. Chem. Phys.* **2001**, *115*, 1213.
(60) Beyer, T. S.; Swinehart, D. F. *Comm. Assoc. Comput. Machines* **1973**, *16*, 379. Stein, S. E.; Rabinovitch, B. S. *J. Chem. Phys.* **1973**, *58*, 2438; *Chem. Phys. Lett*. **1977**, *49*, 1883.
(61) Pople, J. A.; Schlegel, H. B.; Raghavachari, K.; DeFrees, D. J.; Binkley, J. F.; Frisch, M. J.; Whitesides, R. F.; Hout, R. F.; Hehre, W. J. *Int. J. Quantum Chem. Symp*. **1981**, *15* 269. DeFrees, D. J.; McLean, A. D. *J. Chem. Phys*. **1985**, *82*, 333.
(62) Waage, E. V.; Rabinovitch, B. S. *Chem. Rev*. **1970**, *70*, 377.
(63) Chesnavich, W. J.; Bowers, M. T. *J. Phys. Chem.* **1979**, *83*, 900.
(64) Armentrout, P. B. In *Advances in Gas-Phase Ion Chemistry*; Adams, N. G., Babcock, L. M., Eds.; JAI; Greenwich, CT, 1992; Vol. 1, pp 83−119.
(65) See, for example: Sunderlin, L. S.; Armentrout, P. B. *Int. J. Mass Spectrom. Ion Processes* **1989**, *94*, 149.
(66) More, M. B.; Glendening, E. D.; Ray, D.; Feller, D.; Armentrout, P. B. *J. Phys. Chem.* **1996**, *100*, 1605.
(67) Ray, D.; Feller, D.; More, M. B.; Glendening, E. D.; Armentrout, P. B. *J. Phys. Chem.* **1996**, *100*, 16116.
(68) Meyer, F.; Khan, F. A.; Armentrout, P. B. *J. Am. Chem. Soc*. **1995**, *117*, 9740.
(69) See, for example, Figure 1 in: Dalleska, N. F.; Honma, K.; Armentrout, P. B. *J. Am. Chem. Soc*. **1993**, *115*, 12126.
(70) Armentrout, P. B.; Simons, J. *J. Am. Chem. Soc*. **1992**, *114*, 8627.
(71) Frisch, M. J.; Trucks, G. W.; Schlegel, H. B.; Scuseria, G. E.; Robb, M. A.; Cheeseman, J. R.; Zakrzewski, V. G.; Montgomery, J. A., Jr.; Stratmann, R. E.; Burant, J. C.; Dapprich, S.; Millam, J. M.; Daniels, A. D.; Kudin, K. N.; Strain, M. C.; Farkas, O.; Tomasi, J.; Barone, V.; Cossi, M.; Cammi, R.; Mennucci, B.; Pomelli, C.; Adamo, C.; Clifford, S.; Ochterski, J.; Petersson, G. A.; Ayala, P. Y.; Cui, Q.; Morokuma, K.; Malick,

D. K.; Rabuck, A. D.; Raghavachari, K.; Foresman, J. B.; Cioslowski, J.; Ortiz, J. V.; Stefanov, B. B.; Liu, G.; Liashenko, A.; Piskorz, P.; Komaromi, I.; Gomperts, R.; Martin, R. L.; Fox, D. J.; Keith, T.; Al-Laham, M. A.; Peng, C. Y.; Nanayakkara, A.; Gonzalez, C. Challacombe, M.; Gill, P. M. W.; Johnson, B.; Chen, W. Wong, M. W.; Andres, J. L.; Gonzales, C.; Head-Gordon, M.; Replogle, E. S.; Pople, J. A. *Gaussian 98*, revision A.7; Gaussian, Inc.: Pittsburgh, PA, 1998.

(72) Becke, A. D. *J. Chem. Phys.* **1993**, *98*, 5648.

(73) Lee, C.; Yang, W.; Parr, R. G. *Phys. Rev. B* **1988**, *37*, 785.

(74) Foresman, J. B.; Frisch, Æ. *Exploring Chemistry with Electronic Structure Methods*, 2nd ed.; Gaussian: Pittsburgh, PA, 1996.

(75) Boys, S. F.; Bernardi, R. *Mol. Phys.* **1979**, *19*, 553.

(76) Van Duijneveldt, F. B.; van Duijneveldt-van de Rijdt, J. G. C. M.; van Lenthe, J. H. *Chem. Rev.* **1994**, *94*, 1873.

(77) Feller, D.; Glendening, E. D.; Kendall, R. A.; Peterson, K. A. *J. Chem. Phys*. **1994**, *100*, 49881.

(78) Lifshitz, C. *Adv. Mass Spectrom*. **1989**, *11*, 113.

(79) Figures were generated using the output of Gaussian98 geometry optimizations in: *Hyperchem Computational Chemistry Software Package*, Version 5.0; Hypercube Inc.: Gainesville, FL, 1997.

(80) McKenna, A. G.; McKenna, J. F. *J. Chem. Educ*. **1984**, *61*, 771.

(81) Bartlett, R. J. *Annu. Rev. Phys. Chem.* **1981**, *32*, 359.

(82) Hehre, W. J.; Radom, L.; Schleyer, P. v. R.; Pople, J. A. *Ab Initio Molecular Orbital Theory*; Wiley: New York, 1986.

(83) Jones, R. W.; Staley, R. H. *J. Am. Chem. Soc.* **1982**, *104*, 2296.

(84) Magnera, T. F.; Stulik, D. D.; Orth, R. G.; Jonkman, H. T.; Michl, J. *J. Am. Chem. Soc.* **1989**, *111*, 5036.

(85) Bauschlicher, C. W.; Langhoff, S. R.; Partridge, H. *J. Chem. Phys.* **1991**, *94*, 2068. Bauschlicher, C. W.; Partridge, H.; Langhoff, S. R. *J. Phys. Chem.* **1992**, *96*, 3273. Langhoff, S. R.; Bauschlicher, C. W.; Partridge, H.; Sodupe, M. *J. Phys. Chem*. **1991**, *95*, 10677.

(86) Thermal corrections to the values reported by Dalleska et al. were determined here from theoretical calculations at the B3LYP/6-311+G(2d, 2p)//B3LYP/6-31G* level of theory for H_2O, $Cu^+(H_2O)$, and $Cu^+(H_2O)_2$. At this level of theory, the calculated 0 K BDEs of $(H_2O)_{x-1}Cu^+-H_2O$ are 151.7 and 166.2 kJ/mol for $x = 1$ and 2, respectively. The calculated thermal corrections for the reactions $Cu^+(H_2O)_x \rightarrow Cu^+(H_2O)_{x-1} + H_2O$ are $\Delta H_{393} - \Delta H_0 = 3.4 \pm 0.4$ and 3.1 ± 1.1 kJ/mol and $T\Delta S_{393} = 30.2 \pm 2.6$ and 48.1 ± 2.3 kJ/mol for $x = 1$ and 2, respectively.

(87) Walter, D.; Armentrout, P. B. *J. Am. Chem. Soc*. **1998**, *120*, 3176.

(88) Thermal corrections to the values reported by Dalleska et al. were determined here from theoretical calculations at the B3LYP/6-311+G(2d, 2p)//B3LYP/6-31G* level of theory for NH_3, $Cu^+(NH_3)$, and $Cu^+(NH_3)_2$. At this level of theory, the calculated 0 K BDEs of $(NH_3)_{x-1}Cu^+-NH_3$ are 223.5 and 226.0 kJ/mol for $x = 1$ and 2, respectively. The calculated thermal corrections for the reactions $Cu^+(NH_3)_x \rightarrow Cu^+(NH_3)_{x-1} + NH_3$ are $\Delta H_{393} - \Delta H_0 = 6.1 \pm 0.4$ and 3.6 ± 1.3 kJ/mol and $T\Delta S_{393} = 37.7 \pm 0.2$ and 52.5 ± 4.4 kJ/mol for $x = 1$ and 2, respectively.

(89) The difference between the theoretical and experimental values when the molecular constants for the trigonal bipyramidal structure are used to fit the data. The deviation between the theoretical and experimental values is 65.7 kJ/mol when the molecular constants for the ground-state structure are used to fit the data.